JAAS

ROYAL SOCIETY OF CHEMISTRY

PAPER

View Article Online
View Journal

Cite this: DOI: 10.1039/d0ja00493f

Determination of gadolinium MRI contrast agents in fresh and oceanic waters of Australia employing micro-solid phase extraction, HILIC-ICP-MS and bandpass mass filtering

Maximilian Horstmann, [ab] Raquel Gonzalez de Vega, [a] David. P. Bishop, [a] Uwe Karst, [b] Philip A. Doble [a] and David Clases *[a]

Gd-based contrast agents (GBCAs) are frequently administered to patients for magnetic resonance imaging to enhance tissue contrasts. After examination, they are excreted and enter surface waters *via* local wastewater treatment plants' effluents where they lead to anthropogenic Gd anomalies in the environment of metropolitan areas with developed healthcare. This work presents the speciation analysis of GBCAs in water samples from Australia by targeting individual GBCAs in effluent, river and seawater samples obtained from New South Wales (Sydney area), the Northern Territory (Alice Springs) and Victoria (Melbourne area). A method based on hydrophilic interaction liquid chromatography (HILIC) coupled to inductively coupled plasma-mass spectrometry (ICP-MS) provided rapid separation and quantification of four common GBCAs in under three minutes. To improve the sensitivity, ion extraction and transport processes were optimised and the quadrupole mass filter was operated with an increased mass bandpass, decreasing limits of detection to between 18 and 24 ng L^{-1} for individual GBCAs. This allowed detection of Gd-DOTA, Gd-BT-DO3A and Gd-DTPA-BMA at concentrations of up to 160 ng L^{-1} in water samples collected from rivers within the proximity of effluents of local wastewater treatment plants. The analysis of GBCAs in oceanic sea water required the development of a novel automated micro-solid phase extraction (μSPE) method for matrix elimination and analyte pre-concentration enabling the detection of Gd-DOTA and Gd-BT-DO3A.

Received 30th November 2020
Accepted 2nd February 2021

DOI: 10.1039/d0ja00493f

rsc.li/jaas

[a]*The Atomic Medicine Initiative, University of Technology Sydney, 15 Broadway, Ultimo NSW 2007, Australia. E-mail: David.Clases@uts.edu.au*

[b]*University of Münster, Institute of Inorganic und Analytical Chemistry, Corrensstr. 30, 48149 Münster, Germany*

David Clases was born in Paderborn (Germany) in 1989 and developed a passion for the natural sciences in his childhood which stimulated his career of scientific enquiry. After graduating from secondary school in the small town of Neuenheerse in 2009, he commenced his study of Chemistry at the University of Münster (Germany), where he obtained a Bachelor's and Master's degree in 2012 and 2014. Intrigued by Analytical Chemistry as an interdisciplinary science operating at the interface of various fields including medicine, nanotechnology, life- and environmental sciences, he began his PhD studies at the University of Münster under the supervision of Prof. Uwe Karst, and was supported by the German Chemical Industry Association (VCI). As part of a committed and dynamic group, he attained expertise in the application of hyphenated technologies based on inductively coupled plasma-mass spectrometry (ICP-MS) and high-resolution molecular MS. During his studies he was supported by the German Academic Exchange Service to visit the working group of Prof. Philip Doble at the University of Technology Sydney (UTS), Australia, and returned upon the completion of his PhD program in 2017. At UTS, he became a postdoctoral fellow of the German Research Foundation and worked as part of an interdisciplinary team. He has developed an independent research program featuring novel approaches and methods for the characterisation of elemental and proteomic bioindicators and is interested in the analysis of trace elements and emerging nanomaterials in biological and environmental systems. He is a core member of the Atomic Medicine Initiative and, since 2020, employed as a Lecturer of Analytical Chemistry.

Introduction

Worldwide, an increasing number of more than 30 million magnetic resonance imaging (MRI) examinations per year require gadolinium-based contrast agents (GBCAs). Since the introduction of gadopentetate dimeglumine into clinical practice in 1988, a variety of Gd complexes have been developed to improve diagnostic imaging capabilities,[1] from which the most frequently administered chelates are depicted in Fig. 1. After MRI examination, GBCAs are excreted mostly unmetabolised and enter surface waters unaltered *via* effluents of local wastewater treatment plants.[2–5] The frequent use of GBCAs resulted in a substantial discharge into the environment causing anthropogenic Gd anomalies, which are defined as elevated Gd levels relative to other naturally abundant lanthanides. These anomalies are often assessed by normalising concentrations of rare earth elements in waters against a reference material (*e.g.* shales).[6] Anomalies have been detected in waters around metropolitan areas with developed healthcare.[6–13] In Australia, more than 1 million MRI examinations were conducted in 2017 [14,15] and a Gd anomaly was reported in Brisbane (Queensland, Australia) in 2009 and 2010.[16,17]

70% of the Australian population live within ten urban areas,[18] all located on the coast, of which Greater Sydney and Melbourne are the largest. In these areas, approximately 10 million people produce more than 2 billion litres of wastewater daily which is predominantly diffused into the South Pacific Ocean *via* outfalls. However, a small portion of treated wastewater is discharged into surrounding river and creek systems. This complicates speciation analysis as established methods and sampling strategies are often not applicable and quantification and selectivity are impaired due to trace concentrations and complex matrices. Specifically, speciation analysis in saltwater is challenging and requires dedicated pre-treatment as well as detection capabilities to determine individual Gd species. The (eco-)toxicological impact of GBCAs is difficult to estimate due to lack of studies investigating the behaviour of these compounds in the aquatic environment. Research on the fate, bioaccumulation, metabolism, and degradation of Gd complexes is still in an early stage and relies upon extremely sensitive and selective techniques that allow differentiation between species in complex environmental and biological matrices. It has been previously reported by laser ablation-inductively coupled plasma-mass spectrometry (LA-ICP-MS) that Gd from GBCAs may be retained in the body after MRI examination,[19,20] and Lingott *et al.* found that GBCAs in surface waters may be taken up and accumulate in plants and animals.[21]

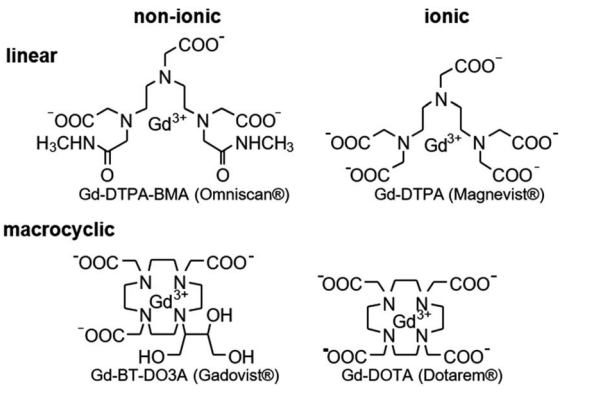

Fig. 1 Structures of the four most administered GBCAs. Top: linear chelates, Gd-DTPA-BMA and Gd-DTPA; bottom: macrocyclic complexes Gd-DOTA and Gd-BT-DO3A.

Positive Gd anomalies in surface and tap waters in densely populated regions were first identified by Bau and Dulski in 1996.[22] Since then, methods for the speciation of Gd have been developed and refined by hyphenation of chromatographic/electrophoretic separation techniques with ICP-MS, which is now a platform technology for trace analyses of soluble element species.[23] Polar or/and ionic species including GBCAs can be separated by ion chromatography,[24] capillary electrophoresis[25] or hydrophilic interaction liquid chromatography (HILIC).[26] HILIC-ICP-MS has been demonstrated to be the gold standard for efficient separation and sensitive detection of GBCAs in environmental samples.[6] Several reviews have been published since the inception of environmental Gd speciation, where the interested reader will find further information, applications and comparisons.[6,27,28] Using HILIC-ICP-MS, Künnemeyer *et al.* investigated the distribution of commonly administered GBCAs in hospital effluents, municipal sewage and wastewater with limits of detection (LODs) as low as 160 ng (Gd) L^{-1}.[29] Telgmann *et al.* investigated the concentrations of these compounds in wastewater and balanced the flux of Gd in a wastewater treatment plant over seven days demonstrating that only 10% of Gd was removed during the treatment process (LOD: 130 ng L^{-1}).[42] The figures of merit of GBCAs have been incrementally improved to enable detection in larger water bodies and complex matrices after significant dilution. Lindner *et al.* analysed GBCAs in surface waters and plant extracts with a reported LOD of 51 ± 11 ng L^{-1}.[30] Using a similar method, Raju *et al.* analysed five GBCAs in surface waters in the Berlin area with LODs of 22 ± 5 ng (Gd) L^{-1}.[31] Birka *et al.* decreased LODs further by employing ultrasonic nebulisation in conjunction with HILIC-ICP-sector field-MS reporting LODs of between 1.3 and 2.2 ng L^{-1} allowing quantitative speciation analysis in drinking water.[32] Similar figures of merit were obtained by Lindner *et al.* who determined GBCAs in tap water samples from the Berlin area (LOD: 1.4–2.4 ng (Gd) L^{-1}).[33] Okabayashi *et al.* recently demonstrated that HILIC separation may be further improved by separating 6 contrast agents in less than 800 seconds reaching detection limits between 3.4 and 22 ng (Gd) L^{-1}.[34] Interestingly, the authors presented a HILIC approach that did not require organic solvents. Decreasing the separation times and consequently accelerating the sample throughput will become increasingly important for larger programs of close-meshed tracing of various samples in larger water bodies. However, while figures of merit incrementally improved over time, methods for speciation analysis in complex matrices like seawater have not been developed.

This work presents a novel automated micro-solid phase extraction (μSPE) method to eliminate complex matrixes and

Table 1 Sampling location, date, time, and description. All samples are associated with WWTP discharges after tertiary treatment

Location	Date, time	Description	Approximate latitude, longitude
1	15/06/2018, 10:44 AM	Downstream of WWTP, (discharge: 32.6 ML day^{-1})	−33.7365, 150.8750
2	15/06/2018, 01:08 PM	Downstream of WWTP, (discharge: 0.9 ML day^{-1})	−33.5750, 150.7167
3	15/06/2018, 10:53 AM	Downstream of WWTP, (discharge: 11.9 ML day^{-1})	−33.7013, 151.0831
4	15/06/2018, 11:20 AM	Downstream of WWTP, (discharge: 24 ML day^{-1})	−33.6673, 150.9210
5	15/06/2018, 03:00 PM	Downstream of WWTP, (discharge: 60 ML day^{-1})	−33.7142, 150.7671
6	15/06/2018, 02:17 PM	Downstream of WWTP, (discharge: 24 ML day^{-1})	−33.7419, 150.6924
7	21/10/2019, 03:11 PM	WWTP effluent (seepage), (discharge: n/a)	−23.7364, 133.8586
8	10/12/2019, 04:34 PM	WWTP effluent diffused in seawater, (discharge: 330 ML day^{-1})	−38.4403, 144.8478

pre-concentrate GBCAs from seawater. Speciation was performed using a rapid HILIC-ICP-MS method which featured improved ion transmission by modifying ion extraction, transport and increasing the mass bandwidth of the quadrupole to improve LODs.

Materials and methods

Ultrapure water was obtained from an Arium® pro system from Sartorius Stedim Biotech (18.2 MΩ, Göttingen, Germany). Acetonitrile (HPLC grade) and ammonium acetate were purchased from Sigma Aldrich (St. Louis MO, U.S.). High purity Gd standards for ICP-MS were obtained at 10 mg L^{-1} from Choice Analytical (Thornleigh, NSW, Australia). All contrast agents were acquired from their respective pharmaceutical suppliers: Magnevist® (Gd-DTPA, 0.5 mol L^{-1}) and Gadovist® (Gd-BT-DO3A, 1.0 mol L^{-1}) from Bayer Pharma AG (Berlin, Germany), Dotarem® (Gd-DOTA, 0.5 mol L^{-1}) from Guerbet SA (Villepinte, France) and Omniscan® (Gd-DTPA-BMA, 0.5 mol L^{-1}) from GE Healthcare (Chalfont St Giles, United Kingdom). 0.45 μm PTFE syringe filters were purchased from Tisch Scientific (North Bend OH, U.S.). Water samples were kept in containers made of polypropylene to avoid adsorption effects of GBCAs. μSPEed cartridges containing μCarb resin (porous graphitic carbon, 3 μm, 250 Å) were obtained from ePrep Pty Ltd (Mulgrave VIC, Australia).

Sample and standard preparation

Samples were collected in 50 mL polypropylene containers previously washed with the sampling matrix. The approximate sampling locations, times and descriptions are listed in Table 1. All samples were filtered to remove larger particles and stored at −20 °C until analysis. For analysis, samples were left at room temperature until thawed and diluted 1 : 10 in eluent. For the construction of calibration curves and species identification, GBCA standards were diluted in water and acetonitrile (eluent composition) to concentrations of 10, 100, 1000 and 10 000 ng L^{-1}. Ultrapure water was used to obtain a blank value. GBCA standards were cross-calibrated using a certified Gd standard for ICP-MS. The standard solutions containing Gd-DTPA, Gd-DOTA, Gd-BT-DO3A and Gd-DTPA-BMA were prepared daily to prevent metal exchange with excess ligands present in the formulations.

For speciation analysis in seawater, an automated μSPE method was developed. Method development was carried out on a digiVOL® Programmable Digital Syringe Driver (ePrep Pty Ltd, Mulgrave VIC, Australia) with μCarb μSPEed® extraction cartridges. For automation, the method was transferred to a Sample Preparation Workstation (ePrep Pty Ltd, Mulgrave VIC, Australia). The workflow for the preparation/pre-concentration of GBCAs from seawater is illustrated in Fig. 2. Syringes made of glass were treated with HNO_3 and flushed with ultrapure water to mitigate carryover of GBCAs. The absence of contaminating GBCAs was regularly checked by preparing and analysing blank solutions. μSPEed® cartridges were conditioned with ultrapure water to activate the carbon surface, loaded with sample volumes between 250 and 1000 μL and eluted with 250 μL (73% acetonitrile, 27% MQ water). The dispensing flow rate for the elution step was optimised to 500 μL min^{-1}, while 1000 μL min^{-1} was used for the conditioning, loading and washing steps. The entire μSPE workflow including syringe cleaning required approximately 15 minutes per sample. As a method blank and medium for spiking experiments, seawater was obtained approximately 30 km outside the metropolitan area of Sydney where no anomaly was expected (−34.1164, 151.1408). Known concentrations of Gd-DTPA, Gd-DOTA, Gd-BT-DO3A and Gd-DTPA-BMA were spiked into the seawater blank and analysed by μSPE and HILIC-ICP-MS to determine recoveries.

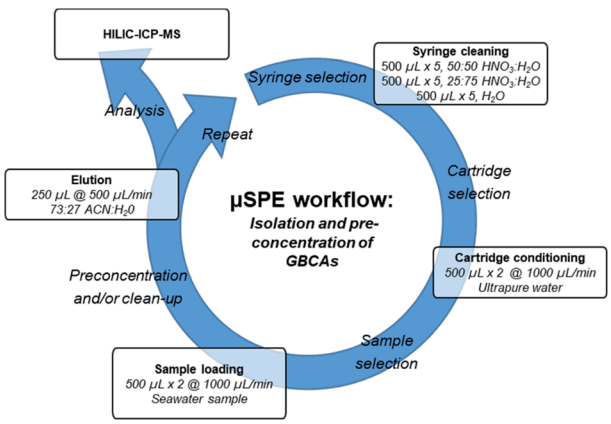

Fig. 2 μSPE workflow for the pre-concentration and clean-up of GBCAs from seawater. Without pre-concentration, the sample loading volume was reduced to 250 μL.

Instrumentation

Chromatographic separations were performed on a 1200 series HPLC system (Agilent Technologies, Santa Clara CA, U.S,) using an Accucore™ HILIC silica LC-column (dimensions 100 × 2.1 mm, particle size 2.6 μm, Thermo Fisher Scientific, Waltham MA, U.S.) equipped with an Accucore™ HILIC defender guard (dimension 10 × 2.1 mm, particle size 2.6 μm). The starting point for the optimisation of the separation method were chromatographic conditions reported by Birka *et al.* in 2013.[26] To accelerate the separation of GBCAs, the dimensions of the chromatographic column were altered (150 × 3 mm, 2.1 μm → 100 × 2.1 mm, 2.6 μm) while increasing the flow rate to 1.1 mL min^{-1}. Furthermore, a higher content of acetonitrile (eluent A: 30% 10 mM ammonium acetate buffer solution in ultrapure water and 10% acetonitrile, eluent B: 70% acetonitrile, isocratic conditions) was used and, the column temperature was set to 40 °C to reduce the backpressure. Different pH values (2–8) of the aqueous eluent (prior to adding acetonitrile) and effects regarding peak shape and separation efficiencies were investigated until finding an optimum at a pH value of 5.3. These optimised parameters reduced the separation time from previously approximately 14 minutes to less than three minutes.[26] The optimum injection volume was determined empirically to be 5 μL while considering peak symmetries and signal to noise ratios. Before each injection, the column was equilibrated for at least 3 minutes.

A 7700 series ICP-MS system (Agilent Technologies) was equipped with platinum cones, cs lenses and a narrow injector torch (1 mm) and operated with MassHunter software (Agilent Technologies). A method with an increased mass bandpass further referred to as bandpass mode was used to improve sensitivity and analysed Gd at 156 amu. The dwell time was set to 100 ms, and 163 amu, 148 amu and 140 amu were monitored additionally to ensure the absence of spectral interferences from other lanthanides. For comparisons, ^{158}Gd was monitored employing a standard method. A 20% oxygen/argon blend was added through a T-piece before the torch to mitigate carbon deposition on the interface (tune value: 25%). A Scott-type double-pass spray chamber (Glass Expansion, Melbourne VIC, Australia) was cooled to −5 °C and a MicroMist™ concentric nebuliser (Elemental Scientific, Omaha NE, U.S.) was used for sample nebulisation. The performance of the ICP-MS instrument was tuned daily with a solution (70 : 30, acetonitrile : water) containing 1 μg L^{-1} Li, Y, Tl and Ce to optimise sensitivity. The CeO/Ce signal was used to determine the oxide rate which was below 5%. The signal to noise ratio for the analysis of Gd was further optimised analysing a diluted 1 μg L^{-1} element standard (70 : 30, acetonitrile : water). The plasma was operated at 1.6 kW and the typical nebuliser gas and make-up gas flow rates were tuned daily to a total gas flow rate of between 0.7 and 0.8 L min^{-1}.

The bandpass mode was developed stepwise by first increasing ion transmission through manipulation of extraction and ion transport conditions. In a second step, the mass bandwidth of the quadrupole mass filter was increased. The bandwidth and mass resolution of a quadrupole are set by the combination of direct current (DC) voltage and RF voltage applied to the four rods. The pairs of RF and DC voltages applied are located on one scan line which is defined *via* a linear function that can be altered by a set of tune parameters. In this case, the scan line function was altered by manipulation of the tune values "Mass Gain" and "Mass Offset". Various combinations of these tune parameters were evaluated for signal to noise ratios of Gd. The optimised experimental parameters for the standard method and the bandpass mode are listed in Table 2.

The advantages of cell gas (He and H_2) were further investigated as part of the tuning process. The flow rates of these gases where optimised by analysing a 1 μg L^{-1} Gd standard diluted in eluent and by comparing the Gd signal to the background monitored outside Gd's mass bandpass. The operation of low cell gas flows reduced the background noise without significantly affecting the sensitivity of Gd leading to improved signal to noise ratios. Furthermore, the application of cell gases appeared to improve the Gd signal stability.

Data handling and figures of merit

Data was processed with Origin 2019 (OriginLab Corporation, Northampton MA, U.S.). Chromatograms were smoothed using a Savitzky–Golay filter over 15 data points. The μSPE recoveries for each compound were determined analysing a 1000 ng L^{-1} GBCA calibration standard mix *via* HILIC-ICP-MS without μSPE, after μSPE (no pre-concentration) and after μSPE with a pre-concentration factor of 4. Column recoveries were calculated by subsequent comparison to flow injection (FI) ICP-MS. The FI method operated the described LC method without the column and was used to determine the peak area for each GBCA standard individually. The peak area determined by FI-ICP-MS was used to normalise the detected area in HILIC-ICP-MS to obtain

Table 2 Instrumental parameters of a standard method (SM) and a method operating the quadrupole with an increased mass bandwidth (bandpass mode (BPM))

Tune mode	SM	BPM
Monitored at [amu]	158	156
Lenses		
Extraction lens 1 [V]	4.0	−80.0
Extraction lens 2 [V]	−150	−5.0
Omega bias [V]	−32	−150
Omega lens [V]	8.6	24.4
Deflect [V]	17.0	20.0
Cell		
He flow [mL min^{-1}]	0	0.5
H_2 flow [mL min^{-1}]	0	0.5
Octopole bias [V]	−6.0	−18.0
Octopole RF [V]	150	13
Energy discr. [V]	4.0	−3.3
Quadrupole		
Mass gain [V]	127	30
Mass offset [V]	129	111

the recoveries. Limits of detection (LODs) and limits of quantification (LOQs) were calculated based on the integral's standard deviation (noise) σ of a calibration blank and the slope (sensitivity, s) of the respective calibration curves (LOD $= 3\sigma/s$, LOQ $= 10\sigma/s$).

Results and discussion

Increasing ion transmission

The sensitivity of ICP-MS is dependent on the ion transport efficiency, which can be increased by several strategies. One involves the use of hard extraction conditions operating the first extraction lens with a highly negative potential and the second extraction lens closer to the ground potential. This increases the kinetic energy of extracted ions, which translates into an increased ion transmission visible as increased sensitivity in ICP-MS. However, background noise and interferences must be monitored closely, as noise usually increases concomitant with ion transmission. If noise increases to a similar extent, signal to noise ratios may deteriorate and LODs increase. The manipulation of extraction potentials is a common approach for sector-field ICP-MS and has also been reported for quadrupole-based ICP-MS, for example in single particle ICP-MS,[35] LA-ICP-MS[36] or gas chromatography (GC)-ICP-MS.[37] However, consideration of the downstream effects is required to optimise the working range of the remaining ion lenses. For example, a curvature of the ion beam is usually induced to eliminate neutral particles and light. Increasing the kinetic energies may require altering electric potentials to maintain and focus of this ion trajectory.

Another strategy to increase ion transmission involves modification of the quadrupole scanning parameters. Similar approaches were previously described for ICP-MS/MS to increase the ion transmission of the first quadrupole, and we recently investigated this concept for single quadrupole ICP-MS instruments.[35,36,38,39] In conventional quadrupole-ICP-MS, m/z are scanned sequentially and therefore, sensitivity is lower for elements with a broad and even isotope distribution when compared with a monoisotopic element. This applies specifically to Gd, which consists of 7 isotopes with abundances between 0.2% and 24.84% as shown in Fig. 3C. Therefore, analysing the most abundant isotope ^{158}Gd limits measurement to a small fraction of the overall Gd, and more than 75% of all

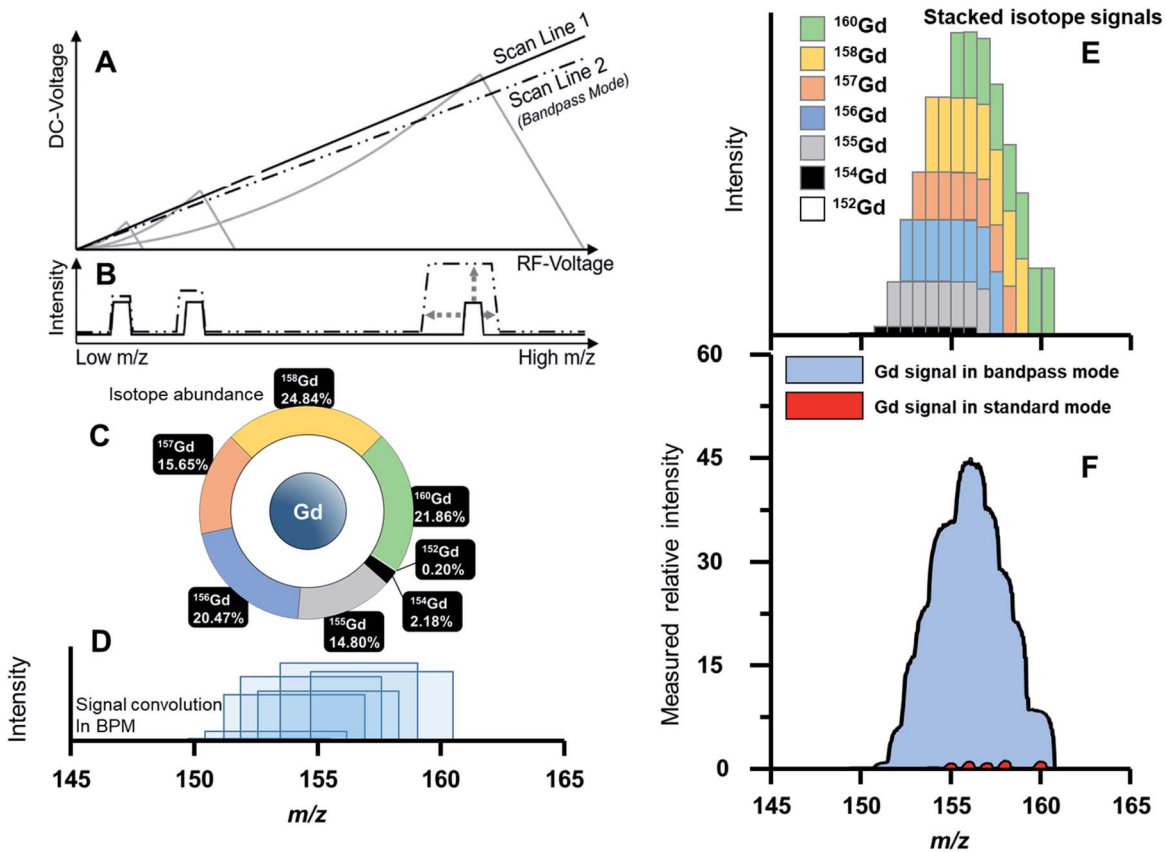

Fig. 3 (A) Stability diagram for three m/z representing low, mid and high masses. Scan line 1 truncates the three stability zones to provide uniform mass resolution and ion transmission over the entire mass scale. Ion transmission and mass resolution may be modified by manipulation of the scan line function (compare scan line 2). (B) Applying scan line 2 increases ion transmission for heavy masses and results in larger mass peak widths. (C) Isotopic abundance of Gd. With a standard mode, highest sensitivity for Gd is achieved at 158 amu. (D) Manipulation of the scan line changes the transmission and mass resolution leading to a convolution of isotopic signals. (E) Stacked simulation of individual isotopic signals. Broad peak widths and signal convolution allows the analysis of several isotopes simultaneously further increasing sensitivity. (F) Comparison of measured mass signals obtained from a standard mode with unit mass resolution and the bandpass mode.

Gd ions transmitted to the quadrupole are subsequently eliminated. Ions with different m/z follow individual trajectories within the quadrupole and the combination of DC voltage and RF voltage applied to the rods determines whether the ion trajectory is stable and focusses onto the detector. Each m/z has a stability zone which can be calculated by solving the Mathieu equations. Fig. 3A shows exemplary stability zones of three m/z in which any combination of DC and RF voltage produce stable trajectories. However, to maintain a consistent (unit) mass resolution and ion transmission, only specific pairs of DC and RF voltages are applied and are located on one line (scan line 1, Fig. 3A).

Modification of the gain and slope of the scan line (compare scan line 2, Fig. 3A) increases transmission of individual high-mass isotopes as exemplified in Fig. 3B. Furthermore, due to the decreasing mass resolution, the mass peak width of each isotope increases to approximately 8 amu causing a convolution of isotopic signals as shown in Fig. 3D. The signal convolution allows transmission of several isotopes simultaneously while applying only one set of RF and DC voltages to the quadrupole, and consequently increases sensitivity further. Fig. 3E shows a simulated mass spectrum demonstrating the isotope signal convolution where individual isotope signals are stacked and Fig. 3F shows a measured mass spectrum of Gd employing a standard method (red) and the bandpass mode (blue). The increased ion transmission of the bandpass mode for individual isotopes and the signal convolution increased sensitivity by a factor of 44 compared against the standard method monitoring the most abundant Gd isotope (^{158}Gd, 24.84%).

For the samples investigated in this study, co-eluting interferences (*e.g.*, other lanthanides or polyatomic interferences) were unlikely. However, depending on the application, large mass bandpass filtering requires consideration of potential spectral overlaps of targeted isotopes and potentially interfering compounds. This may become increasingly relevant when other lanthanide anomalies are present as for example described by Kulaksiz and Bau.[40] Increasing sensitivity by increasing the mass bandwidth of the quadrupole decreases mass selectivity. While the loss of unit mass resolution contributes to the improved ion transmission and isotope signal convolution which increases sensitivity, it becomes more difficult to distinguish Gd from other adjacent lanthanides and polyatomic interferences. At the same time, background noise may increase and limit the gain in signal to noise ratios and improvement in LODs. It is noteworthy that the mass bandwidth broadens asymmetrically. For example, increasing the mass bandwidth of an isotope with m/z 159 from 1 amu to 8 amu did not produce a mass signal that was symmetrically centred around 159 amu with ±4 amu. Instead, the mass signal was shifted towards lower masses with signal boundaries at approximately 152.5 and 160.5 amu. This is a direct consequence of asymmetric stability zones shown in Fig. 3A and is relevant for consideration of potential isobaric and polyatomic interferences, which may affect accuracy when operating a large mass bandpass. In this case, monitoring Gd at 156 amu achieved the highest sensitivity and prevented interferences from lighter lanthanide isotopes like ^{153}Eu. However, a spectral overlap with isotopes from ^{159}Tb, ^{162}Er, ^{156}Dy, ^{158}Dy, ^{160}Dy, ^{161}Dy and ^{162}Dy was possible and was investigated to ensure accuracy. The impact of Er and Dy on the Gd signal was evaluated by monitoring 163 amu additionally to 156 amu. To recognise the potential impact of lighter isotopes forming polyatomic interferences (*e.g.*, ^{140}Ce^{16}O), 140 amu and 148 amu were also monitored. Furthermore, all samples investigated in the framework of this study were first analysed *via* FI-ICP-MS to screen for lanthanides using a standard method and no significant signals for any lanthanide potentially interfering with Gd were found. To prevent potential polyatomic interferences and to reduce background noise, He and H_2 were used as cell gases.

Speciation analysis in surface waters

A standard mix containing the four GBCAs was diluted to 100 ng L^{-1} and analysed by HILIC-ICP-MS employing a standard method and the bandpass mode, respectively. Fig. 4A (blue) shows the resulting chromatogram demonstrating rapid separation of all four GBCAs in less than three minutes. The figures of merit of both methods and each GBCA are shown in Table 3. The R^2 values were determined as a measure of linearity and were at least 0.9997. The column recovery was 104% for Gd-DTPA, 105% for Gd-DOTA, 70% for Gd-BT-DO3A and 89% for

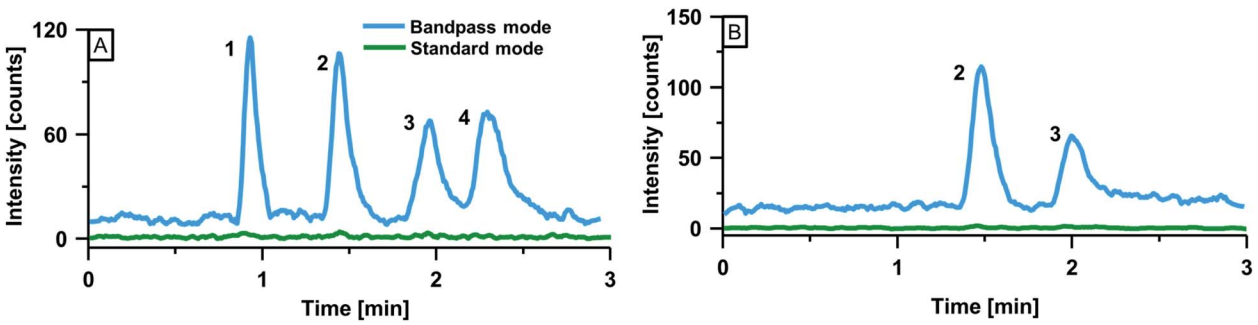

Fig. 4 (A) Separation of a 100 ng L^{-1} mix containing the 4 most frequently administered GBCAs ((1) Gd-DTPA, (2) Gd-DOTA, (3) Gd-BT-DO3A, (4) Gd-DTPA-BMA). Two methods were used for signal acquisition: a standard method with soft extraction conditions (green), and a bandpass mode method (blue). (B) Chromatographic separation of a riverine sample obtained in the Sydney region (location 4) employing the standard and bandpass mode.

Table 3 Figures of merit for each GBCA and method. A standard method (SM) and a method operating the quadrupole in bandpass mode (BPM) were compared

Unit		Sensitivity, Cts L ng^{-1}	Noise, Cts	LOD, ng L^{-1}	LOQ, ng L^{-1}	R^2, —
Gd-DTPA	SM	0.12	4.3	110	350	0.9997
	BPM	6.0	40	20	67	0.9999
Gd-DOTA	SM	0.14	5.3	120	390	1.0000
	BPM	6.6	39	18	60	0.9999
Gd-BT-DO3A	SM	0.12	4.8	120	410	0.9999
	BPM	5.5	45	24	81	1.0000
Gd-DTPA-BMA	SM	0.17	5.3	100	320	0.9999
	BPM	7.4	52	21	71	0.9999

Gd-DTPA-BMA. The LODs and LOQs of GBCAs acquired with the standard method were between 100–120 ng L^{-1} and 320–410 ng L^{-1}, respectively, and were in agreement with previous studies using similar instrumentation.[4,29] Accordingly, individual GBCAs were not detected analysing a 100 ng L^{-1} calibration standard as shown in Fig. 4A (green). The manipulation of ion extraction and transport as well as operating the quadrupole in bandpass mode increased sensitivity by a factor of between 43 and 50 for the individual GBCA while increasing background noise by a factor of less than 10 (compare Table 3). The increases in sensitivity were in line with values obtained analysing Gd *via* standalone ICP-MS as shown in Fig. 3F. Consequently, LODs and LOQs decreased to 20 and 67 ng L^{-1} for Gd-DTPA, 18 and 60 ng L^{-1} for Gd-DOTA, 24 and 81 ng L^{-1} for Gd-BT-DO3A and 21 and 71 ng L^{-1} for Gd-DTPA-BMA allowing the detection and quantification of all four GBCAs as shown in Fig. 4A (blue). The improved figures of merit were crucial for the detection of GBCAs in surface waters in the Sydney area (Australia). Sample locations 1–5 (compare Table 1) were located within the greater Sydney region. Most wastewater (approximately 88%) of Sydney is diffused offshore and only a fraction is released into local waterways. Consequently, concentrations of GBCAs are low and speciation analysis required sensitive methods. Fig. 4B shows the speciation analysis of a surface water obtained from a creek in northwest Sydney (location 4). While the standard method was not able to detect GBCAs, operating hard extraction conditions and improving ion transmission by increasing the mass bandpass of the quadrupole allowed the quantification of Gd-DOTA (130 ± 5 ng L^{-1}) and the additional detection of Gd-BT-DO3A (<LOQ). Determined species and concentrations for all locations are listed in Table 4.

Table 4 Concentrations of GBCAs detected in freshwater samples. All concentrations are given in ng L^{-1}. GBCAs below the LOD were labelled as "not detected (n.d.)" and GBCAs determined between the LOD and LOQ are labelled as "<LOQ"

Location	Gd-DTPA	Gd-DOTA	Gd-BT-DO3A	Gd-DTPA-BMA
1	n.d.	<LOQ	160 ± 5	n.d.
2	n.d.	n.d.	n.d.	n.d.
3	n.d.	n.d.	n.d.	n.d.
4	n.d.	130 ± 5	<LOQ	n.d.
5	n.d.	<LOQ	n.d.	n.d.
6	n.d.	<LOQ	110 ± 3	100 ± 1
7	n.d.	60 ± 3	n.d.	n.d.

Speciation analysis in seawater

The majority of wastewater in Australian coastal cities is diffused into the Pacific Ocean *via* deep water ocean outfalls. The speciation analysis of GBCAs in seawater is confounded by the high salt content limiting the applicability of HILIC-ICP-MS. Fig. 5 (top) shows the analysis of a standard mix containing four GBCAs at 1 μg L^{-1} in seawater (red). It is evident that the high ionic strength of the seawater matrix interfered with the separation mechanism in HILIC and prevented the speciation of

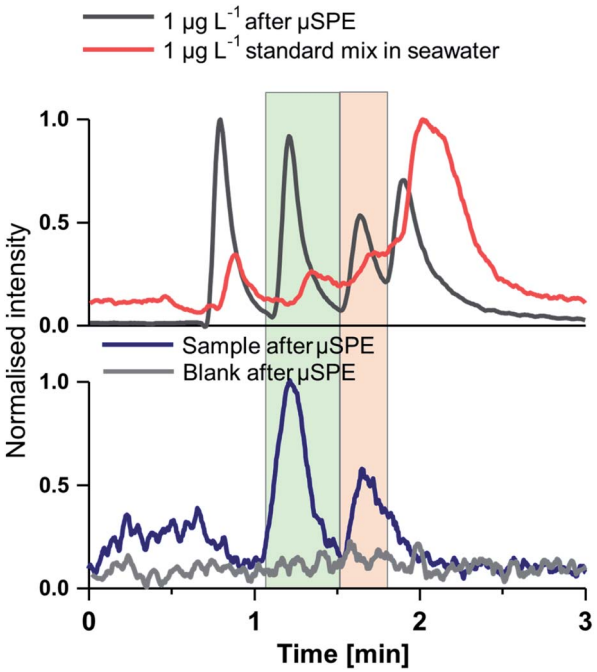

Fig. 5 Top: HILIC-ICP-MS (bandpass mode) of seawater spiked with a GBCA calibration standard mix with (grey) and without (red) previous μSPE (elution order: (1) Gd-DTPA, (2) Gd-DOTA, (3) Gd-BT-DO3A, (4) Gd-DTPA-BMA). Bottom: analysis of coastal seawater obtained at location 8. Seawater obtained from rural Sydney was used as blank.

Table 5 Recoveries after μSPE without pre-concentration and with a pre-concentration factor of 4

Gd species	μSPE recovery, %	μSPE recovery after pre-concentration, %
Gd-DTPA	99.8 ± 8.6	73.1 ± 12.9
Gd-DOTA	99.2 ± 1.3	93.5 ± 5.4
Gd-BT-DO3A	99.2 ± 3.0	94.1 ± 11.7
Gd-DTPA-BMA	99.0 ± 1.0	90.0 ± 8.1

individual Gd species. Activated carbon was previously reported to partially remove GBCAs from water resources.[41] In this work, activated carbon was obtained in μSPEed® cartridges to achieve automated extraction from seawater. As proof of principle, four GBCAs were spiked into seawater without Gd anomaly (1 μg L^{-1}), and subsequently extracted using a fully automated method employing a Sample Preparation Workstation (ePrep Pty Ltd) and analysed by HILIC-ICP-MS operating the quadrupole in bandpass mode. Fig. 5 (top) shows the resulting chromatogram (grey) and compares it to the direct analysis of the same GBCAs in the spiked seawater (red). The extraction method was crucial to remove the matrix and allowed the separation of individual GBCAs for quantification. The recovery of the developed μSPE method was determined analysing spiked seawater samples and was between 99.0 and 99.8%. This method was further investigated for its potential to pre-concentrate GBCAs. A 4-fold pre-concentration factor was achieved with recoveries between 73.1 and 94.1. The recoveries for each GBCA are listed in Table 5. Fig. 5 (bottom) shows the chromatogram of a sample obtained in coastal seawater within the proximity of a wastewater effluent (location 8). Two signals corresponding to Gd-DOTA and Gd-BT-DO3A were detected and calibrated at 180 ± 34 and 140 ± 36 ng L^{-1}.

Conclusion

This work presents the speciation analysis of GBCAs in the Australian environment. Increasing ion extraction and transport and increasing the mass bandwidth of the quadrupole mass filter improved sensitivity by factors of between 43 and 50 relative to a standard method, and decreased LODs and LOQs to between 18 and 24 ng L^{-1} and 60 and 81 ng L^{-1} respectively, for the four investigated GBCAs Gd-DTPA, Gd-DOTA, Gd-BT-DO3A and Gd-DTPA-BMA. These improvements allowed the detection and quantification of GBCAs (between 60 and 160 ng L^{-1}) in Australian riverine water samples. A novel automated μSPE method allowed matrix elimination and detection of individual species (Gd-DOTA and Gd-BT-DO3A) in seawater for the first time. The recovery of the GBCAs was between 99.0 and 99.8% without pre-concentration and between 73.1 and 94.1% with four-fold pre-concentration. These methods have the potential to sufficiently improve figures of merit to trace GBCAs in surface and coastal seawater to monitor the discharge and distribution of GBCAs in the marine environment. The rapid HILIC separation and the fully automated μSPE workflow have further potential for high throughput analyses and to facilitate close-meshed speciation analysis in larger water bodies.

Author contributions

The manuscript was written through contributions of all authors. All authors have given approval to the final version of the manuscript.

Conflicts of interest

There are no conflicts to declare.

Acknowledgements

This research is supported by the UTS Seed Funding scheme. DPB is supported by an Australian Research Council Discovery Early Career Researcher Award DE180100194. PAD is supported by Australian Research Council Discovery Project Grant DP190102361. DC is funded by the Deutsche Forschungsgemeinschaft (DFG, German Research Foundation) – 417283954. The authors acknowledge the support by ePrep Pty Ltd, Victoria, Australia.

References

1 J. Lohrke, T. Frenzel, J. Endrikat, F. C. Alves, T. M. Grist, M. Law, J. M. Lee, T. Leiner, K. C. Li, K. Nikolaou, M. R. Prince, H. H. Schild, J. C. Weinreb, K. Yoshikawa and H. Pietsch, *Adv. Thermoelectr.*, 2016, **33**, 1–28.
2 P. Verlicchi, A. Galletti, M. Petrovic and D. BarcelÓ, *J. Hydrol.*, 2010, **389**, 416–428.
3 S. Kulaksiz and M. Bau, *Appl. Geochem.*, 2011, **26**, 1877–1885.
4 L. Telgmann, C. A. Wehe, J. Künnemeyer, A. C. Bülter, M. Sperling and U. Karst, *Anal. Bioanal. Chem.*, 2012, **404**, 2133–2141.
5 K. Kümmerer and E. Helmers, *Environ. Sci. Technol.*, 2000, **34**, 573–577.
6 D. Clases, M. Sperling and U. Karst, *TrAC, Trends Anal. Chem.*, 2018, **104**, 135–147.
7 S. Kulaksiz and M. Bau, *Earth Planet. Sci. Lett.*, 2007, **260**, 361–371.
8 P. Möller, P. Dulski, M. Bau, A. Knappe, A. Pekdeger and C. Sommer-von Jarmersted, *J. Geochem. Explor.*, 2000, **69–70**, 409–414.
9 M. Rabiet, F. Brissaud, J. L. Seidel, S. Pistre and F. Elbaz-Poulichet, *Chemosphere*, 2009, **75**, 1057–1064.
10 F. Elbaz-Poulichet, J. L. Seidel and C. Othoniel, *Water Res.*, 2002, **36**, 1102–1105.
11 M. Bau, A. Knappe and P. Dulski, *Chem. Erde*, 2006, **66**, 143–152.
12 T. Ogata and Y. Terakado, *Geochem. J.*, 2006, **40**, 463–474.
13 P. A. Rinck and R. N. Muller, *Eur. Radiol.*, 1999, **9**, 998–1004.
14 *Australia: Total population from 2014 to 2024 (in millions)*, IMF, online: https://www.statista.com/statistics/263740/total-population-of-australia/, 2019.
15 OECD, in *Health at a Glance*, 2019, p. 193.

16 M. G. Lawrence, *Mar. Pollut. Bull.*, 2010, **60**, 1113–1116.
17 M. G. Lawrence, C. Ort and J. Keller, *Water Res.*, 2009, **43**, 3534–3540.
18 *Australian Bureau of Statistics*, 2018.
19 D. Clases, S. Fingerhut, A. Jeibmann, M. Sperling, P. Doble and U. Karst, *J. Trace Elem. Med. Biol.*, 2019, **51**, 212–218.
20 M. Birka, K. S. Wentker, E. Lusmöller, B. Arheilger, C. A. Wehe, M. Sperling, R. Stadler and U. Karst, *Anal. Chem.*, 2015, **87**, 3321–3328.
21 J. Lingott, U. Lindner, L. Telgmann, D. Esteban-Fernández, N. Jakubowski and U. Panne, *Environ. Sci.: Processes Impacts*, 2016, **18**, 200–207.
22 M. Bau and P. Dulski, *Earth Planet. Sci. Lett.*, 1996, **143**, 245–255.
23 D. P. Bishop, D. J. Hare, D. Clases and P. A. Doble, *TrAC, Trends Anal. Chem.*, 2018, **104**, 11–21.
24 P. Hajós, D. Lukács, E. Farsang and K. Horváth, *J. Chromatogr. Sci.*, 2016, **54**, 1752–1760.
25 J. Künnemeyer, L. Terborg, S. Nowak, L. Telgmann, F. Tokmak, B. K. Krämer, A. Günsel, G. A. Wiesmüller, J. Waldeck, C. Bremer and U. Karst, *Anal. Chem.*, 2009, **81**, 3600–3607.
26 M. Birka, C. A. Wehe, L. Telgmann, M. Sperling and U. Karst, *J. Chromatogr. A*, 2013, **1308**, 125–131.
27 J. Rogowska, E. Olkowska, W. Ratajczyk and L. Wolska, *Environ. Toxicol. Chem.*, 2018, **37**, 1523–1534.
28 L. Telgmann, M. Sperling and U. Karst, *Anal. Chim. Acta*, 2013, **764**, 1–16.
29 J. Künnemeyer, L. Terborg, B. Meermann, C. Brauckmann, I. Möller, A. Scheffer and U. Karst, *Environ. Sci. Technol.*, 2009, **43**, 2884–2890.
30 U. Lindner, J. Lingott, S. Richter, N. Jakubowski and U. Panne, *Anal. Bioanal. Chem.*, 2013, **405**, 1865–1873.
31 C. S. K. Raju, A. Cossmer, H. Scharf, U. Panne and D. Lück, *J. Anal. At. Spectrom.*, 2010, **25**, 55–61.
32 M. Birka, C. A. Wehe, O. Hachmöller, M. Sperling and U. Karst, *J. Chromatogr. A*, 2016, **1440**, 105–111.
33 U. Lindner, J. Lingott, S. Richter, W. Jiang, N. Jakubowski and U. Panne, *Anal. Bioanal. Chem.*, 2015, **407**, 2415–2422.
34 S. Okabayashi, L. Kawane, N. Y. Mrabawani, T. Iwai, T. Narukawa, M. Tsuboi and K. Chiba, *Talanta*, 2021, **222**, 121531.
35 S. Meyer, R. Gonzalez de Vega, X. Xu, Z. Du, P. A. Doble and D. Clases, *Anal. Chem.*, 2020, **92**, 15007–15016.
36 D. Clases, R. Gonzalez de Vega, S. Funke, T. E. Lockwood, M. Westerhausen, R. V. Taudte, P. A. Adlard and P. Doble, *J. Anal. At. Spectrom.*, 2020, **35**, 728–735.
37 D. Clases, M. Ueland, R. Gonzalez de Vega, P. Doble and D. Pröfrock, *Talanta*, 2021, **221**, 121424.
38 L. Balcaen, G. Woods, M. Resano and F. Vanhaecke, *J. Anal. At. Spectrom.*, 2013, **28**, 33–39.
39 D. P. Bishop, D. Clases, F. Fryer, E. Williams, S. Wilkins, D. J. Hare, N. Cole, U. Karst and P. A. Doble, *J. Anal. At. Spectrom.*, 2016, **31**, 197–202.
40 S. Kulaksiz and M. Bau, *Earth Planet. Sci. Lett.*, 2013, **362**, 43–50.
41 M. P. Elizalde-González, E. García-Díaz, M. González-Perea and J. Mattusch, *Environ. Sci. Pollut. Res.*, 2017, **24**, 8164–8175.
42 L. Telgmann, C. A. Wehe, M. Birka, J. Künnemeyer, S. Nowak, M. Sperling and U. Karst, *Environ. Sci. Technol.*, 2012, **46**, 11929–11936.